INTERFEROMETRIC SYNTHETIC APERTURE SONAR ENSEMBLE ESTIMATE COHERENCE

Shannon-Morgan Steele

Kraken Robotics

ABSTRACT

Interferometric Synthetic Aperture Sonar (InSAS) measurements are noisy and typically require multiple estimates of the scene depth to constrain the vertical uncertainty (vertical resolution). Many InSAS systems sacrifice horizontal resolution for vertical resolution by utilizing spatial averaging. In previous work, we demonstrated a technique termed Seamless SAS that can form multiple observations of each image pixel, allowing us to substantially reduce the amount of spatial averaging required by supplementing it with ensembles. This paper is an extension of our previous work, focusing on furthering our theoretical understanding of the ensemble technique by analyzing the coherence between adjacent pings and synthetic aperture image strips collected by the Kraken Miniature Interferometric Synthetic Aperture Sonar (MINSAS).

Index Terms— SAS, Sonar, Interferometry, Bathymetry, Ensemble, Coherence

1. INTRODUCTION

InSAS simultaneously measures seabed backscatter and relative seabed depth utilizing two or more vertically separated interferometric receivers. The interferometric vertical uncertainty (vertical resolution) is dependent on the interferometric signal coherence, where even small reductions in coherence from unity will significantly impact the depth estimate [1]. To produce an interferogram of the image scene with low vertical uncertainty, multiple estimates of the scene relative depth are required [1]. Existing techniques for obtaining multiple interferometric estimates either lower the interferogram horizontal resolution (spatial averaging and sub-banding), require additional hardware (multiple frequency bands, or three or more vertically separated arrays) [1], or impose extra survey time and sensitivity to temporal inchoherence (multi-pass) [2, 3, 4]. Many InSAS systems cannot incorporate additional hardware and must balance a trade off between horizontal and vertical resolution due to spatial averaging or sub-banding the imaging bandwidth. Centimetric resolution in all three dimensions is desirable for a variety of applications such as mine hunting [5] or hydrographic surveys where strict requirements of resolution must be met [6].

In previous work, we described Seamless SAS processing and demonstrated Seamless SAS as a viable technique to achieve centimetric resolution in all three dimensions without modifying the SAS hardware or survey routine [7]. With the ensembles produced by Seamless SAS, spatial averaging can be reduced to two samples. This yielded a spatial resolution improvement from 25 cm to 6 cm while maintaining centimetric vertical resolution on both featureless (primarily speckle) images and complex cluttered images (featuring small and large objects) [7]. The overlapping SAS imaging strips used for the ensemble estimate include significant redundancy, and thus the effective number of looks (estimates) used in the ensemble will not necessarily be equivalent to the nominal number of looks used. The effective number of looks analysis in our previous work showed that the effective number of looks is dependent on the spatial averaging used, and for the MINSAS, the horizontal averaging should be limited to centimeter resolutions for the effective number of looks to be similar to the nominal number of looks. Given the high redundancy between the ensemble estimates, one would expect low independence between looks, and thus these results may not seem intuitive. In this paper we present a set of analyses that show the coherence between pings and synthetic apertures are relatively low, and thus more independent than might initially be assumed.

2. METHODS

2.1. Seamless SAS processing

SAS imagery is typically produced using beamformers that partition the imaging space into large rectangular blocks that extend tens of metres in the along track direction with a small overlap between immediate neighbour blocks. An alternative, albeit less efficient method, is to process data on a ping-to-ping basis with the image space partitioned into narrow rectangular blocks. The resulting image strips significantly overlap and can be mosaicked into a continuous SAS image of any desired length (up to one survey leg) in the along track using the vehicle Inertial Navigation System. These significantly overlapping image strips can also be used to form an ensemble of interferometric estimates for the same image pixel. A detailed explanation of the Seamless SAS processing can be

979-8-3503-0864-8/24/$31.00

found in [7]. For the MINSAS we typically obtain about three ensemble estimates per pixel.

2.2. Image strip coherence analyses

In interferometric processing, the coherence typically refers to the coherence between the two or more rows of vertically separated receivers. Here, we analyze the coherence of a single receiver row in the along track direction, which we can use as a proxy for the ensemble sample independence. The coherence can be computed as the magnitude of the complex correlation at zero lag [8]. Coherence analyses before and after Seamless SAS image strip processing will be presented. We computed the ping to ping coherence to measure the coherence between pings before SAS processing. At each ping the data received by the receivers were matched filtered and summed like a conventional side scan sonar. The coherence between consecutive pings was then calculated over a sliding range window, and repeated for all pings used to form the image. After Seamless SAS image strip processing we computed the two-dimensional strip to strip coherence. The two-dimensional strip to strip coherence is the magnitude of the two-dimensional coherence between two consecutive, co-registered beamformed SAS image strips, computed over a two-dimensional sliding window. A two-dimensional map of the strip to strip coherence where each pixel is the magnitude of the two-dimensional cross correlation was formed. To help understand the scale dependency of the coherence results the ping to ping and strip to strip coherence were computed at 18 cm and 60 cm resolution, which correspond to three and ten times the ensemble interferometry map resolution, respectively.

2.3. Study Data

All data utilized in this study was collected using a Kraken MINSAS 180. The MINSAS 180 consists of two rows of interfermotric receivers, each approximately 1.6 m in length. The MINSAS has a 40 kHz bandwidth with a centre frequency of 337 kHz. With SAS processing the MINSAS is capable of achieving along track and across track resolutions of 3 cm in real-time and 2 cm with post processing. Depending on the environmental and operational settings the MINSAS can image to a max range of 200 m and an area coverage rate of up to 4 km^2/h.

The coherence analysis described in Section 2.2 will be repeated for seven different MINSAS surveys conducted in a variety of operational and environmental settings, which we will refer to as study areas A-H. The operational and environmental settings of each study area are summarized in Table 1. Most study areas included multiple areas of interest; the areas of interest are indicated in the description column of Table 1. For example, study area D has four areas of interest: a boulder field (majority of seabed area is covered with boulders), scattered boulders (occasional boulders on an otherwise featureless seabed), featureless (speckle dominated) seabed, and a barge sitting on the seabed. Figure 1 shows examples of the seabed textures and compositions used to describe the areas of interest in Table 1. In total 20 areas of interest were used for this coherence analysis. Before processing, an array phase calibration was computed and applied to each study area. The phase calibration procedure includes range-variant corrections for bistatic geometry and phase curvature of the received wavefield (including phase offsets due to array mounting errors) [9]. Each study area was also analysed to determine a suitable max range with high enough SNR to compute the coherence.

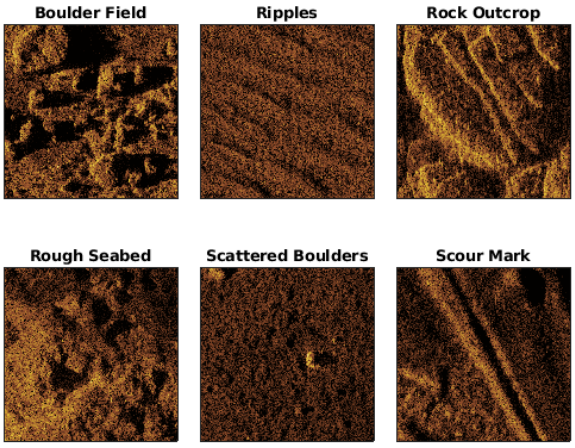

Fig. 1. Sample images for seabed textures and compositions described in Table 1. Each image shows a 10 x 10 m portion of a SAS image.

3. RESULTS AND DISCUSSION

Figure 2 shows the ping to ping and strip to strip coherence probability density functions (pdf) over all of the areas of interest. At the 18 cm resolution we see both the ping to ping and strip to strip coherence pdfs follow a Gaussian distribution. The ping to ping and strip to strip pdfs at 60 cm resolution have a more complex distribution. This complex distribution arises from significant differences in the coherence distribution of the twenty different areas of interest. Figure 3 shows the strip to strip coherence pdfs from a selection of individual areas of interest. At 60 cm resolution it appears each pdf is complex and seems to be heavily impacted by environmental parameters. Speckle dominated seabeds tend to have distributions skewed more strongly towards lower coherence, while seabeds dominated by clutter tend to have flatter distributions trending towards a more uniform distribution and higher coherence overall, likely caused by the tendency of

Study Area	Vehicle Speed ($\frac{m}{s}$)	Altitude (m)	Pulse Length (ms)	Sound Speed ($\frac{m}{s}$)	Location	Description
A	1.73	20	10	1486	Virginia/North Carolina	1: Shipwreck with clutter (small and large objects) 2: Featureless (speckle dominated) seabed
B	1.89	15	10	1479	Grand Banks, NL	1: Rock Outcrop 2: Featureless (speckle dominated) seabed
C	2.10	13	7	1455	Grand Banks, NL	1: Small ripples (0.55 m wavelength), 2: Large ripples (1.75 m wavelength), 3: Boulder field
D	2.35	12	3	1448	Woodside, Halifax	1: Boulder field, 2: Scattered boulders, 3: Featureless seabed, 4: Large Object (Barge)
E	1.79	20	10	1445	Offshore NS	1: Rock outcrop, 2: Boulder field, 3: Shipwreck, 4: Rough seabed/boulders
F	1.90	15	5	1468	Holyrood, NL	Shallow water on 16% sloping seabed with clutter (small objects)
G	1.89	17	10	1455	Halifax Harbour	Seabed with scour marks
H	2.35	12	3	1448	Bedford, Halifax	1: Seabed with scour marks 2: Rough seabed 3: Speckle dominated seabed

Table 1. Summary of environmental and operational parameters for all study areas.

clutter objects to scatter coherently. The environmental dependency of the coherence measurements reduces as the window over which the coherence is computed decreases. For example, at the 60 cm window size the coherence of the wreck (located at approximately 60-100 m across track) is clearly higher than the surrounding seabed; however, with 18 cm window size there is no discernible difference between the clutter and seabed coherence (Figure 4). This is consistent across all 20 areas of interest. At the 18 cm resolution the pdfs for all the areas of interest follow a Gaussian distribution with no statistically significant difference in their distributions. The Z-test statistic between coherence distributions for all the different areas of interest are below 0.4 and 0.5, for the ping to ping and strip to strip coherence measurements, respectively. The rest of our analysis will focus only on the 18 cm coherence estimates, as it appears the window size of the coherence analysis at 60 cm causes the coherence measurement to be heavily impacted by environmental and operational factors.

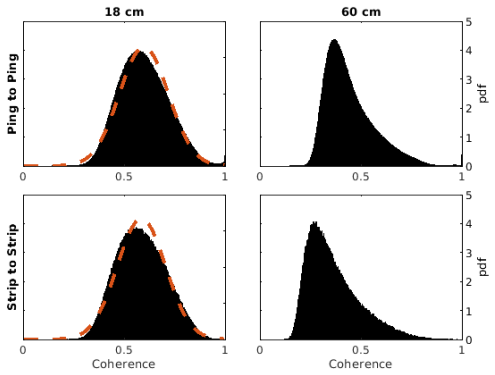

Fig. 2. Probability density functions (pdfs) with Gaussian fit (red dashed lines) for ping to ping (top row) and strip to strip (bottom row) coherence, computed over 18 cm (left column) and 60 cm (right column) windows.

Since there is no significant difference in the coherence distributions amongst all the areas of interest at the 18 cm window size, we can combine them all into one distribution (as done in Figure 2) and compute a Gaussian fit to the data (red dashed line in Figure 2). The Gaussian fit indicated the average coherence to be 0.598 ± 0.122 before SAS processing and 0.589 ± 0.120 after SAS processing. The cumulative density functions (cdfs), presented in Figure 5 show 95 % and 96 % of samples have a coherence less than 0.8 before and after SAS processing, respectively. Completely dependent samples would have a coherence of one and completely independent samples a coherence of zero. Therefore the synthetic apertures used for Seamless SAS processing are partially independent. The partially independent samples produced by the Seamless SAS apertures can be combined into an ensemble interferometry estimate that is equivalent to an effective number of independent looks less than the number of apertures used in the ensemble.

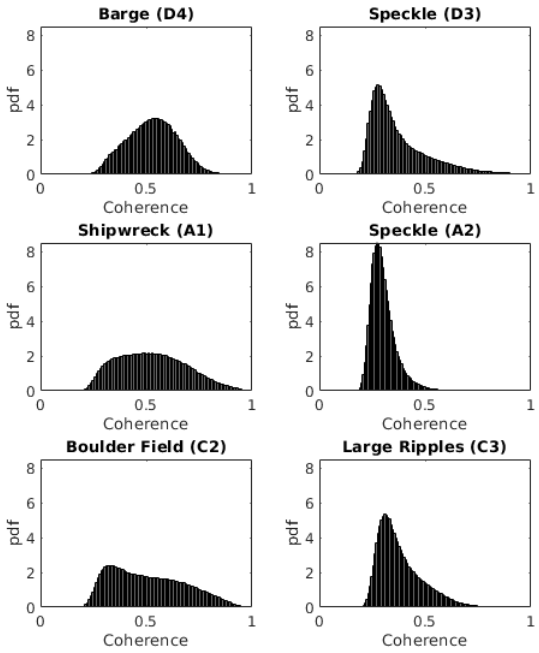

Fig. 3. Strip to strip coherence pdfs computed over 60 cm windows for a selection of the areas of interest described in Table 1.

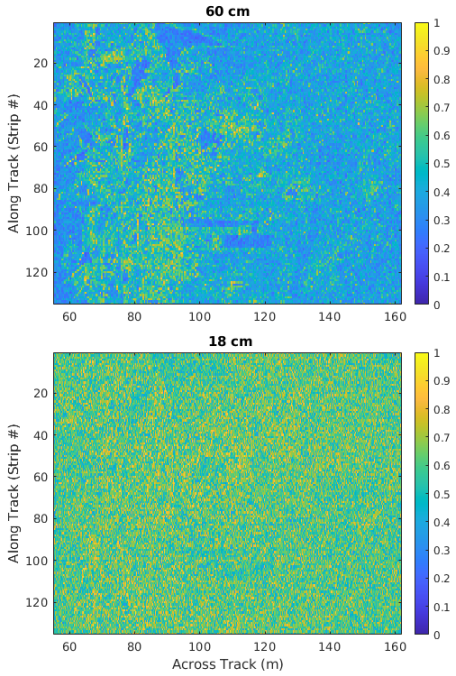

Fig. 4. Strip to strip coherence maps of a SAS image of a shipwreck surrounded by clutter (study area A1), computed over 60 cm windows (top) and 18 cm windows (bottom).

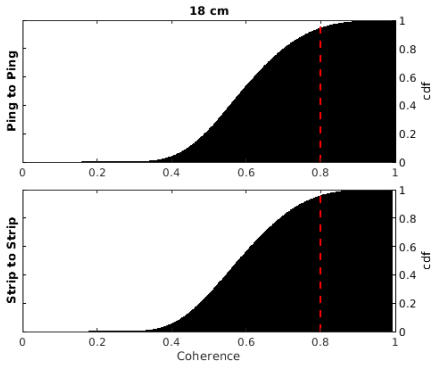

Fig. 5. Ping to ping (top) and strip to strip (bottom) coherence cdfs computed over 18 cm sliding windows. Red dashed line indicates the proportion of samples that have a coherence of less than 0.8.

4. CONCLUSION

This paper presented a coherence analysis of interferometic SAS ensembles. We found a significant scale dependency of the coherence, where the coherence at 60 cm is heavily impacted by environmental conditions. At 18 cm the coherence is consistently Gaussian distributed with no significant difference in the coherence distributions between all the areas of interest. From the twenty areas of interest we found the average coherence to be 0.598 ± 0.122 before SAS processing and 0.589 ± 0.120 after SAS processing. While the Seamless SAS image strips are not completely independent, they are significantly less coherent than one would expect them to be, considering they differ by just one ping. Each Seamless SAS image strip cannot be considered a completely independent sample or look for an ensemble interferomery estimate. However, they can be considered a partially independent sample that, when combined with ensemble interferometric processing, are equivalent to an effective number of independent looks, which will be less than the number of apertures used in the ensemble. These effective looks can be used in conjunction with spatial averaging to achieve interferometry estimates with high vertical and horizontal resolution.

5. REFERENCES

[1] Philip J. Barclay, *Interferometric synthetic aperture sonar design and performance*, Ph.D. thesis, University of Canterbury, Christchurch, New Zealand, 2006.

[2] Jeremy Dillon and Vincent Myers, "Baseline estimation for repeat-pass interferometric synthetic aperture sonar," in *EUSAR 2014; 10th European Conference on Synthetic Aperture Radar*, 2014.

[3] Jeremy Dillon and Vincent Myers, "Coherence estimation for repeat-pass interferometry," in *2014 Oceans - St. John's*, 2014.

[4] Ruggero De Paulis, Claudio Maria Prati, Silvia Scirpoli, Fabio Rocca, Alessandra Tesei, P. A. Sletner, Stefano Biagini, Piero Guerrini, Francesco Gasparoni, Cosmo Carmisciano, and Marina Locritani, "Sas multipass interferometry for monitoring seabed deformation using a high-frequency imaging sonar," *OCEANS 2011 IEEE - Spain*, pp. 1–10, 2011.

[5] Franck Florin, Franck Fohanno, Isabelle Quidu, and Jean-Philippe Malkasse, "Synthetic aperture and 3d imaging for mine hunting sonar," *Undersea Defence Technology (UDT) Europe 2004, Nice France*, 2004.

[6] "International hydrographic organization standards for hydrographic surveys s-44 edition 6.0.0," 2020.

[7] Shannon-Morgan Steele and Richard Charron, "Interferometric synthetic aperture sonar bathymetry maps using ensembles," *Institute of Acoustics Proceedings: 5th international conference on Synthetic Aperture in Sonar and Radar*, vol. 45, 2023.

[8] R. Touzi, A. Lopes, J. Bruniquel, and P.W. Vachon, "Coherence estimation for sar imagery," *IEEE Transactions on Geoscience and Remote Sensing*, vol. 37, no. 1, pp. 135–149, 1999.

[9] Jeremy Dillon and Shannon-Morgan Steele, "In situ array calibration for synthetic aperture sonar," in *Global Oceans 2020: Singapore – U.S. Gulf Coast*, 2020, pp. 1–5.